Forward Micro-inverter with Primary-Parallel Secondary-Series Multicore Transformer

D. Meneses, O. García, P. Alou, J. A. Oliver, R. Prieto, J. A. Cobos.

I. Introduction

Series connection of PV modules to supply a voltage-fed grid-connected inverter is the conventional solution to overcome the low voltage generated by PV arrays. However, the energy yield of these configurations is affected by mismatches between PV modules and partial-shading, especially in residential applications. Distributed maximum power point tracking (DMPPT) architectures improve the energy harvesting capability by means of a module integrated converter (MIC) [1,2].

In DMPPT systems, applications for DC-DC converters as well as for DC-AC inverters have been proposed. In both cases a high voltage boost is required to interface the low output voltage provided by the PV module to the grid. Despite nonisolated solutions have been presented for both DC-DC [3] and AC-module applications [4], the use of a transformer is widespread providing flexibility and compliance with safety standards [5-10].

Current-fed converters, such as boost-type configurations, are proper choices for high step-up configurations. However, a voltage-fed second stage is required due to the inability of these converters to generate voltages lower than their input voltage. Therefore, these converters are widely used in DMPPT or as a DC-DC stage in two-stage inverters [6-8].

In AC-module applications, single-stage flyback inverter is a commonly used topology [9,10] due to its simple structure. The most of the presented configurations are operating in DCM, thus behaving as a current source dependent on the grid voltage.

Voltage-fed converters have also been used as step-up DC-DC converters in two-stage inverters [11,12]. In [13] a single-stage inverter based on a boundary mode controlled forward converter is presented. Since these topologies are buck-derived, the required turn ratio for an adequate voltage boosting is larger than in the flyback inverter or in the current-fed converters.

The large turns ratio complicates the achievement of good coupling between primary and secondary, thus resulting in high leakage inductance and extra losses in the windings [11]. Precisely, in [11] three different configurations for a 1:11 transformer are analyzed and compared in terms of leakage inductance, resonance frequency, series and parallel resistance and converter efficiency. One of the proposed configurations consists of 11 unity turns ratio transformers parallel-input and series-output connected. This split configuration is not only of great interest to reduce the leakage inductance, but also provides advantages in terms of thermal management and cost reduction, if the elementary transformer is seen as a generic unit for mass production. Furthermore, the possibility to split the converter in several smaller converters with unity ratio transformer is suggested.

The use of parallel interleaved converters is common in low-voltage high-current applications. Besides the reduced current stress in the components, the size of the magnetics components can be reduced and the efficiency at light load is improved by dynamically connecting or disconnecting phases [10,14]. The current sharing in the interleaved parallel configuration in the primary side of an isolated coupled inductor boost converter is explored in [5]. However, the secondary side is connected in series thus improving the voltage gain of the proposed solution. A similar configuration is used in [15]. In this case the primary side is paralleled by duplicating the transformer and the primary switches, which are synchronously driven. The same solution with integrated planar magnetics is presented in [16]. The similar concept has been also applied for a full-bridge converter [17].

Regarding the forward converter, the parallel interleaved approach cannot operate with duty cycle higher than 0.5 when both converters share the output inductor [18]. In [19] a series-rectifier configuration, with a common active clamp configuration, is presented to overcome the duty cycle limitation. In the previous solution, there are always two diodes in the current path. In [20] the current path is reduced to one diode by a different configuration of the secondary side diodes, while remaining the capability of operating the converter with duty cycle higher than 0.5.

This paper presents a forward inverter with multiple transformer primary-parallel secondary-series connected for AC-module application. In section II the operation of the converter is analyzed as well as the main design aspects. In section III transformer cores are selected based on the area

product parameter for configurations with different number of phases. These configurations are compared in terms of size, losses, leakage inductance and resonance frequency. Finally, simulation and experimental results for a 2-transformer and an 8-transformer configurations with 45V and 120W input are provided to validate the presented analysis.

II. PROPOSED SOLUTION

A forward micro-inverter based on inductor current boundary mode control (BCM) is presented in [13]. Besides the zero-crossing distortion derived from the selected analog power factor corrector controller, the main design consideration is the power transformer.

Since the forward converter is a buck derived topology the required turns ratio to achieve a proper interfacing between the low PV module voltage and the grid is large. As a result, the obtained efficiency is low (approximately 80%). Furthermore, the design of the transformer requires an oversized core in order to achieve a compromise between the leakage inductance and the resonance frequency.

A. *Proposed Topology*

Fig. 1 shows the proposed forward topology. The solution, derived from a classical forward converter consists of several transformers which are parallel connected in the primary side and series connected in the secondary side.

The primary switches are synchronized and sinusoidally modulated following the boundary mode control strategy to generate a rectified sinusoidal current, which is unfolded in a line frequency switched bridge to inject unity power factor current to the grid. The parallelization in the primary side reduces the current stresses in both switches and primary windings of the transformer.

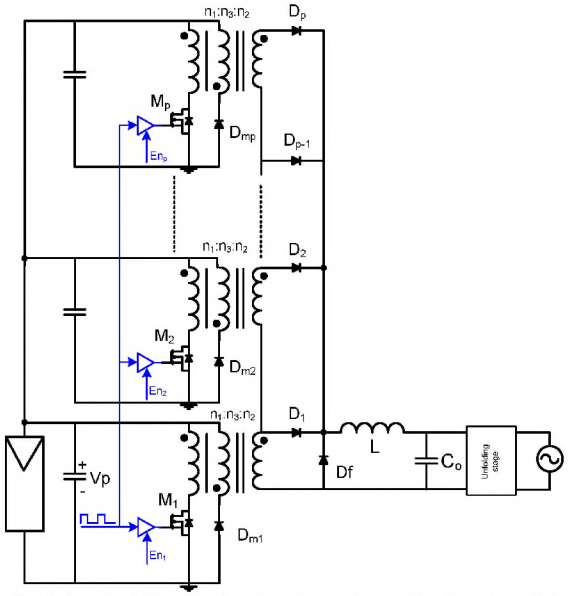

Fig. 1. Proposed forward micro-inverter topology with primary-parallel secondary-series connected transformers.

The series connection in the secondary side allows achieving the grid voltage using transformers of lower turns ratio. Therefore, the primary to secondary coupling at each transformer can be significantly improved and parameters such as leakage inductance can be reduced. Furthermore, the number of active phases is modulated based on the grid voltage, thus achieving a variable transformer ratio.

B. *Operation Principle*

The operation of the topology can be divided in two intervals as the classical forward converter operating in boundary or continuous conduction mode. Fig. 2 and Fig. 3 show the main ideal waveforms of the proposed solution as well as the operation modes for a four transformer converter, when two (Fig. 2) and four (Fig. 3) phases are active. As it can be observed, the common cathode configuration of the secondary diodes together with the synchronized control strategy make that only one of the secondary side diodes is in the current path at each moment.

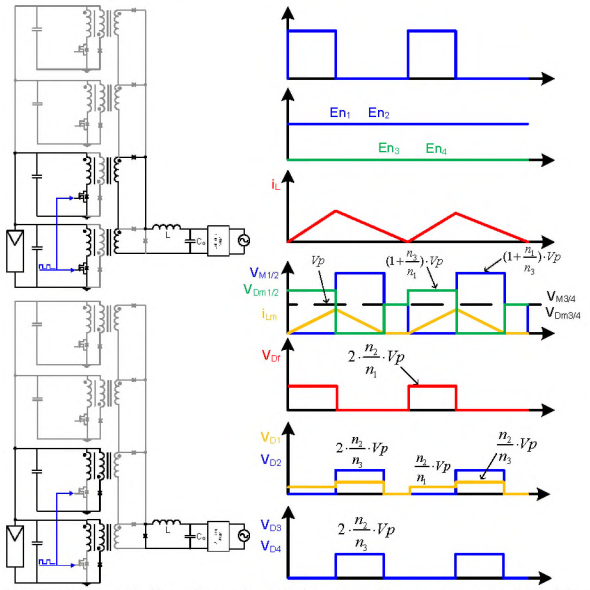

Fig. 2. Ton and Toff configurations (left) and main waveforms (right) of the proposed converter when two phases are active.

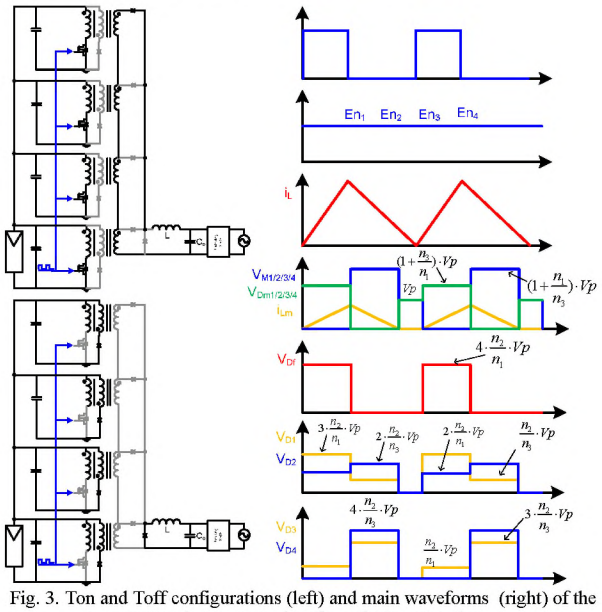

Fig. 3. Ton and Toff configurations (left) and main waveforms (right) of the proposed converter when four phases are active.

C. Voltage Gain

Due to the secondary side configuration the voltage applied to the inductor depends on the number of active phases during the magnetization while the demagnetization is always done with the output voltage, in the same manner than in classical forward converter. Therefore the voltage gain can be expressed as:

$$Vo = n \cdot m \cdot d \cdot Vp \tag{1}$$

Where 'n' is the primary to secondary turns ratio (n_2/n_1) of each transformer and 'm' is the number of active phases.

D. Inductor value and variable frequency operation

The applied boundary mode control strategy ensures the injection of unity power factor current to the grid. However, the converter is operated with variable frequency and a trade-off between the chosen maximum frequency and the necessary inductance value (RMS currents inside the circuit) must be achieved, for a given power level (2). With regard to the minimum operation frequency of the converter, it can be calculated as in (3), where 'p' is the total number of phases.

$$f_{\max} = \frac{V_{O\_RMS}^{\ 2}}{2 \cdot L \cdot Po} \tag{2}$$

$$f_{\min} = \left(1 - \frac{V_{O\_pk}}{n \cdot p \cdot Vp}\right) \cdot f_{\max} \tag{3}$$

E. Component Stress

Since the operation of the proposed converter is the same than in a classical forward converter, the primary side component voltage stress in the proposed solution is the same than in the classical topology. However, the parallel operation of the converter reduces the current stress due to the current sharing. As an example, Fig. 4 shows the current peak value of the switch M1 in Fig. 1 for one phase (blue) and four phases (red) operation. As a consequence the RMS value in a line period is reduced, even more in the phases which are not active during the whole line period, such as switch 4 in Fig. 4.

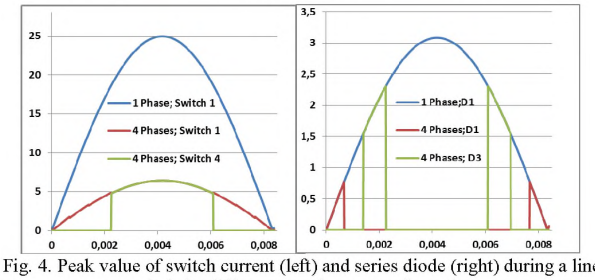

Fig. 4. Peak value of switch current (left) and series diode (right) during a line period, for different transformer configuration.

With regard to the secondary side, only one of the diodes is in the current path at each moment and due to the applied series configuration, the current stress is drastically reduced in the secondary side diodes (Fig. 4, right).

The voltage stress for the freewheeling diode and the 'i-th' series diode (D_i in Fig. 1) of the secondary side can be calculated according to (4) and (5), where 'p' is the total number of transformers for the selected configuration.

$$V_{KA\_FW} = p \cdot \frac{n_2}{n_1} \cdot Vp \tag{4}$$

$$V_{KA\_Di} = \max[(p-i) \cdot \frac{n_2}{n_1} \cdot Vp, i \cdot \frac{n_2}{n_3} \cdot Vp] \tag{5}$$

F. Semiconductor Losses Estimation

The switches and diodes losses are estimated following the same procedure. In the case of the primary switches, both the RMS value and the voltage-current product when the switch is turned off are calculated at each switching cycle. Afterwards, those calculated values are used to compute the average in a line period. The same procedure is used for the mean values of the diode currents. The losses can be calculated according to (6) and (7):

$$P_{Switch\_i} = 1.6 \cdot R_{DSon} \cdot \left(\frac{1}{k} \cdot \sum_{k,T_{grid}} I_{M1\_RMS\_k}\right)^2 + \frac{1}{2} \cdot \left(\sum_{k,T_{grid}} V_{OFF\_i} \cdot I_{M1\_pk}\right) \cdot t_{fall} \cdot f_{grid} \tag{6}$$

$$P_{Diode\_j} = V_{F\_j} \cdot \frac{1}{k} \cdot \sum_{k,T_{grid}} I_{Dj\_avg\_k} \tag{7}$$

G. Demagnetization ratio

In the forward inverter presented in [13] both primary windings are used for energy transfer and transformer reset, according to the grid voltage polarity. Therefore, the demagnetization ratio is fixed to 1. However, in the presented solution the unfolding stage is not integrated in the forward stage and the primary windings are dedicated either for transfer energy or transformer reset.

Therefore, the transformer reset can be performed with a different ratio than 1. As a consequence, the maximum allowable duty cycle can be higher than 0.5, thus decreasing the primary to secondary turn ratio. However, the voltage stress of the switch and the current stress of the demagnetization diode are modified.

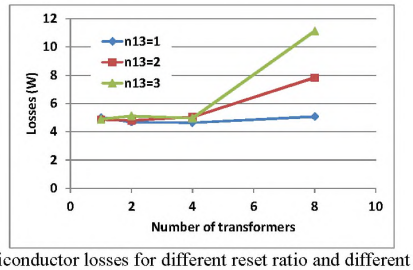

Fig. 5. Semiconductor losses for different reset ratio and different number of phases.

The losses calculations presented above are used to assess the influence of a reset ratio different than 1. Fig. 5 shows the total losses in the semiconductors for different number of phases when the reset ratio (n13 = n1:n3) is changed from 1 to 3. As shown in Fig. 5 the increase in the reset ratio, implies an increase in the losses, regardless the number of phases. As a conclusion, a unitary reset ratio will be considered in the analysis of the proposed topology.

H. Primary to secondary turn ratio and number of phases

Due to the unitary transformer reset ratio, the duty cycle is limited to 0.5 to ensure a proper demagnetization. Considering an extra limitation of 90% of 0.5 and according to (1), the primary to secondary turn ratio of each transformer can be expressed as a function of the total number of utilized phases ('p'):

$$n(p) = \frac{V_{o\_pk}}{p \cdot 0.45 \cdot Vp} \tag{8}$$

According to (8) the product of the primary to secondary turns ratio per phase (n2/n1) and the number of phases keeps constant.

I. *Input Capacitor (Power decoupling)*

In the case of AC-module applications, the fact that the PV module provides a low voltage together with the low allowable ripple to ensure a high maximum power point tracking (MPPT) efficiency, implies that a large capacitance is required (2mF@45V, for a 8.5% of voltage ripple [21]). As a consequence, in most of the cases an electrolytic capacitor is used, which may reduce the life span of the solutions.

In the proposed topology this capacitance can be distributed among the phases, thus reducing the capacitance to use in each of the phases. Therefore, increasing the number of phases allows a change in the technology of the used capacitors, i. e. an increase in the life span of the solution as well as a height reduction.

III. Transformer Size and Losses Estimation

In this section the selection of the appropriate core is analyzed using the area product parameter. Based on this selection, different transformers are designed and compared in terms of size, losses, leakage inductance and resonance frequency.

A. *Core Selection Based on Area Product Parameter*

The area product parameter (Ap) is defined as the product of the cross section (Ae) and the window area (Aw) of a given core. The area product parameter can be used to estimate the volume and weight as well as the power-handling ability of a core [22] and it is easy to obtain from the core datasheets provided by the manufacturers. This parameter can be calculated according to (9):

$$Ap = Ae \cdot Aw = \frac{Vp \cdot d_{\max}}{n_1 \cdot B_{\max} \cdot f_{\min}} \cdot \frac{1.2 \cdot (n_1 \cdot I_{RMS1} + n_2 \cdot I_{RMS2})}{k_w \cdot J_{\max}} \tag{9}$$

Where 'kw' is the window filling factor and 'Bmax' and 'Jmax' are the maximum allowed flux and current density, respectively. Only the primary and secondary windings currents are considered and an extra 20% is used to estimate the demagnetization windings.

Fig. 6 shows the estimated RM cores for different configurations (1, 2, 4 and 8 transformers) of the proposed topology for an output power of 120W, input voltage of 45V and to be connected to the US grid. The transformer turns ratio for each phase is calculated according to (8) and the RMS currents of the windings over a line period are calculated using the same procedure than for the losses calculation. A filling factor of 0.3 and a maximum current density of 600A/cm2 are utilized. The maximum allowed flux density has been limited to a 65% of the saturation limit for the core material 3C90.

B. *Volume, Area and Height*

Based on the selected cores using the area product parameter (Fig. 6), the maximum height as well as the total surface and volume of the transformers considering the bobbin has been calculated for each configuration.

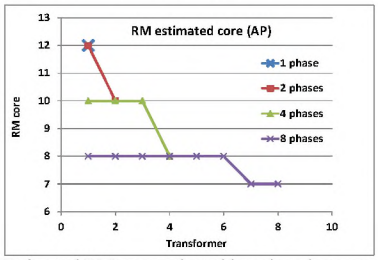

Fig. 6. Estimated RM cores selected based on the area product.

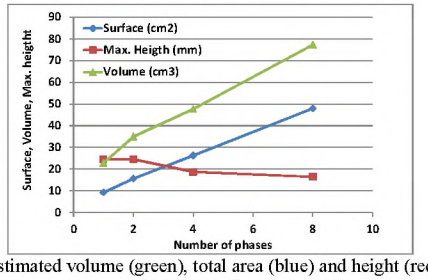

Fig. 7. Estimated volume (green), total area (blue) and height (red) of the selected transformers.

As shown in Fig. 7, the total estimated area increases with the number of phases as well as the total volume of the transformers. However, the maximum estimated height decreases as the number of phases increase. It must be noticed that in AC-module application the converter is attached to the back side of a PV module and, therefore, the available area is large. Furthermore, the low height allows mounting the micro-inverter in the frame of the solar module [23].

C. *Transformer Comparison*

A design of each transformer for the different proposed configurations has been developed based on the selected cores shown in Fig. 6. The software tools PExprt and PEmag have been used in order to compare the designs in terms of losses, resonance frequency and leakage inductance.

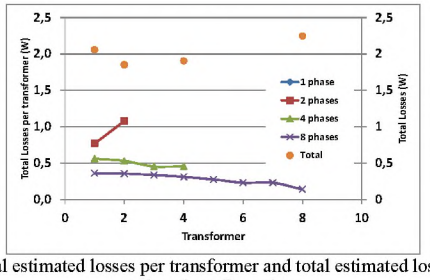

Fig. 8. Total estimated losses per transformer and total estimated losses for the analyzed configurations.

Fig. 8 shows the total estimated losses for each transformer and for the whole set of transformers. The winding losses are estimated with PExprt using the finite elements (FE) models generated by PEmag. However, the core losses are estimated by using both the average frequency and the average of the flux density variation in a grid line period in the Steinmetz equation.

As shown in Fig. 8 the total losses are similar for the analyzed configurations. However, as the number of transformers increases the losses are more spread contributing to an easier thermal management.

Parasitic effects, such as the parasitic capacitance or leakage inductance, can disturb the proper operation of the converter.

Using the finite elements analysis, the parasitic capacitance of the primary winding has been estimated. This value is used together with the obtained magnetizing inductance to estimate the transformer resonance frequency.

As show in Fig. 9, the resonance frequency of the analyzed solutions increases when the turn ratio gets closer to the unity, i. e. with the number of phases. Furthermore, the designs for configurations with one or two transformers need to be optimized since the operation frequency range is close to the obtained resonance frequency. As a result, bigger cores need to be used reducing the primary turns thus increasing the core losses and penalizing the leakage inductance.

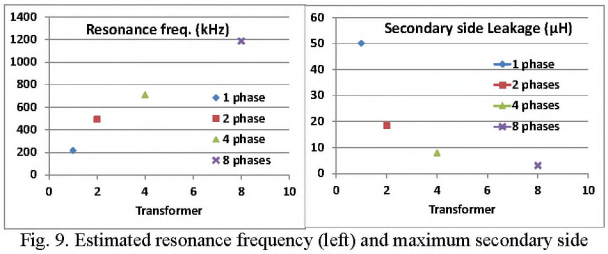

Fig. 9. Estimated resonance frequency (left) and maximum secondary side leakage inductance (right) of the analyzed designs.

Another advantage of the proposed topology is that an increase in the number of transformer decreases significantly the leakage inductance of the designed transformers as shown in Fig. 9.

IV. Discontinuous Conduction Mode Operation

According to (2) and (3) the operating frequency range increases when the delivered power decreases, thus increasing the switching losses and jeopardizing the inverter efficiency (Fig. 10). Therefore, discontinuous conduction mode (DCM) operation is used in order to improve the efficiency at light load operation (Fig. 10)

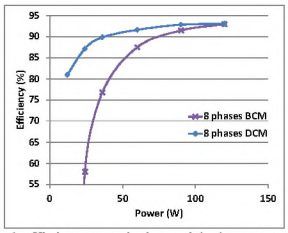

Fig. 10. Estimated efficiency variation with the output power for an 8-transformer configuration at DCM and BCM operation.

In DCM operation a unity power factor can be achieved if the duty cycle is varied according to (10), which can be derived from considering the mean value of the inductor current proportional to the output voltage [24,25].

$$d(t)=\frac{v_o(t)}{Vp}\cdot\sqrt{\frac{k_{DCM}}{n\cdot\left(n-\frac{v_o(t)}{Vp}\right)}};k_{DCM}=\frac{2\cdot L\cdot f_{sw}}{V_{o\_RMS}}\cdot P_o \quad (10)$$

As an advantage of the DCM operation the inverter does not require a current sensing since the necessary duty cycle variation to achieve unity power factor can be obtained using the input and output voltage information.

V. Estimated Efficiency

The previously presented transformer losses for the different configurations together with the estimated losses following the procedure introduced above and the inductor losses are used to estimate the efficiency. It must be noticed that all the analyzed configurations have the same output inductor.

Fig. 11 shows how the estimated efficiency changes with the delivered power as well as the conduction mode of operation (left) and the estimated CEC efficiency [26] for the considered configurations(right).

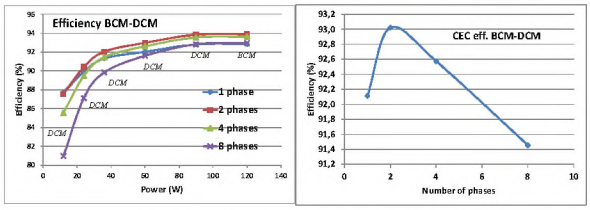

Fig. 11. Efficiency estimation for the analyzed configurations.

As it can be seen the estimated efficiency is similar for the analyzed configurations. However, the calculation excludes the effect of leakage inductance which is expected to be significant for the configurations of 1 or 2 transformers, since the turns ratio is far from unity.

VI. Experimental Results

Two prototypes of 2-transformer (best expected efficiency) and 8-transformer (lowest transformer height) have been designed and built to interface a 45V, 120W PV module to the US grid (110V@60Hz). Both prototypes have the same output filter (L=400µH, C=1µF), same primary switch (IRFS4410PbF) and same secondary side diode (C3D02060E). The transformers of each prototype are designed according to the selected core for phase 1 in Fig. 6 (1:4-RM12 and 1:1-RM8 respectively).

Fig. 17 shows the 2-transformer prototype with dimensions of 174x193mm. In the case of the 8-transformer prototype (Fig. 18) the dimensions are 254x173mm. Despite the 8-transformer configuration has lower transformer profile, the maximum height in both converters is fixed by the 30mm of the inductor ETD34 core. In terms of decoupling capacitor, the 8-transformer solution uses SMD ceramic capacitor while the 2-transformer circuit uses both ceramic and electrolytic capacitors.

The presented results were obtained with a DC source in the input and the grid connection is emulated with an AC voltage source in parallel with a resistor. The DC input voltage was changed accordingly to the NA-F121 PV module voltages for a temperature of 50°C for the different irradiation (power) levels, emulating the MPPT behavior (Table 1).

Fig. 12 shows the full-load BCM operation (left) and DCM operation at 30% of the maximum power (right). The AC waveforms for the 2-transformer configuration are presented in Fig. 13 for BCM full-load (left) and DCM half-load (right). Fig. 14 presents high-frequency waveforms of the tested configurations. The left side shows the current (Ch4) and voltage applied to the filter (Ch2) as well as the driving signal for phase 4 (Ch1) when this phase is turned off for the BCM operation of the 8-transformer configuration. Right image presents the driving signals (Ch3,4) and the inductor current (Ch2) for the grid peak voltage in the DCM operation of the 2-transformer prototype.

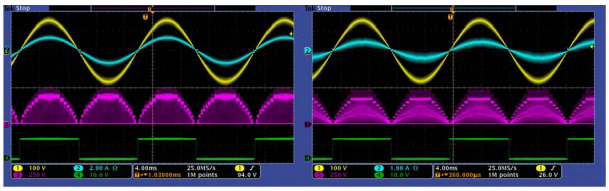

Fig. 12. 8-transformer AC operation for BCM full-load (left) and DCM 30% load (right)

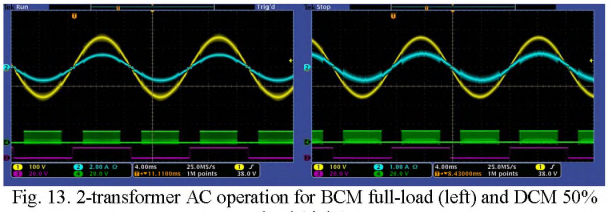

Fig. 13. 2-transformer AC operation for BCM full-load (left) and DCM 50% load (right)

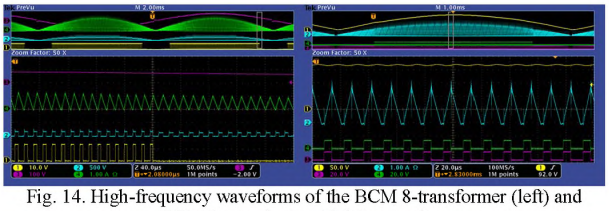

Fig. 14. High-frequency waveforms of the BCM 8-transformer (left) and DCM 2-transformer (right) operation.

The efficiency and THD results obtained are presented in Fig. 15 and Fig. 16 respectively. In terms of THD, the 8-phases transformer configuration presents a better performance in the whole power range, being under the 5%. In terms of efficiency both converters present similar performance with a CEC efficiency around 92.4%. The 8-transformer configuration performs better in the full-load range while the 2-transformer one is better in the light-load power levels. Fig. 19 and Fig. 20 show the thermal response of both prototypes at full load, being better the thermal management of the 8-transformer prototype.

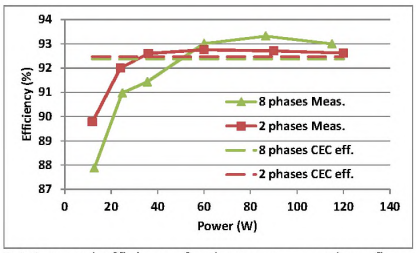

Fig. 15. Measured efficiency for the two proposed configurations.

VII. CONCLUSION

This paper introduces a multiphase primary-parallel secondary-series forward inverter for photovoltaic AC-module application. The operation of the proposed topology is analyzed providing the main design features. The influence of the number of phases in the topology is analyzed in order to get the best trade-off between size, losses, leakage inductance and resonance frequency of the transformers. In addition a DCM operation is introduced to overcome the increase in the operation frequency at light load. Based on the analysis, two prototypes of 2 and 8 transformers were built. Both converters present the same weighted efficiency of 92.4%, however the 8-transformer solution provides better efficiency in the full-load range. Despite in the proposed designs the inductor limits the minimum height of both solutions, the low-profiled 8-transformer configuration allows using ceramic capacitors and offers better THD and thermal management capabilities.

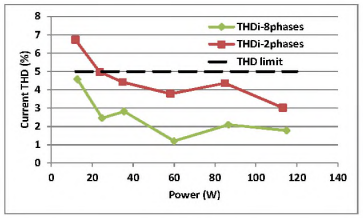

Fig. 16. Current THD measured for the two proposed configurations.

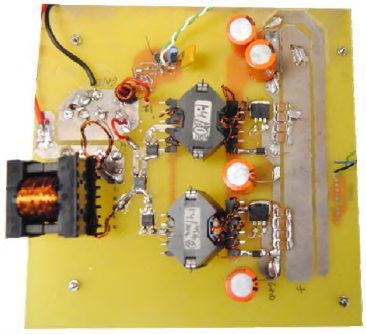

Fig. 17. PCB layout of the 2-transformer configuration

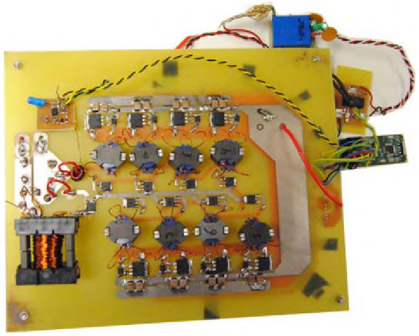

Fig. 18. PCB layout of the 8-transformer configuration.

P(W)	VMPP(V)@50°C
120	45
90	42,8
60	41,6
36	40,67
24	40,2
12	39,7

Table 1. PV voltages of the NA-F121 module for 50°C.

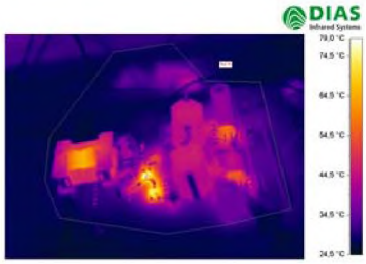

Fig. 19. Thermal image of the 2-transformer prototype.

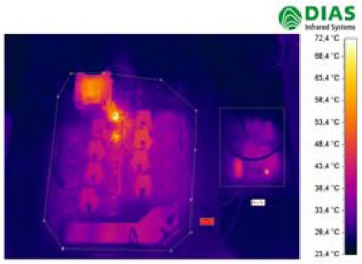

Fig. 20. Thermal image of the 8-transformer prototype.